RESEARCH PAPER

Real-time label-free detection of DNA hybridization using a functionalized graphene field effect transistor: a theoretical study

Sheida Bagherzadeh-Nobari ⬤ ·
Reza Kalantarinejad

Abstract Detection of DNA hybridization with high sensitivity and accuracy plays a major role in clinical diagnosis and treatment. Despite intense experimental studies of graphene field effect transistor as DNA hybridization detector, the mechanism of detection and changes in the electrical properties of the device is not investigated in detail. To this end, we have investigated an armchair graphene nanoribbon (AGNR) interconnected between gold electrodes as a detector of DNA hybridization. Using non-equilibrium Green's function method and density functional theory, the effect of 1-pyrenebutanoic acid succinimidyl ester (PBASE) linker, probe, and target DNA on the electrical properties of the device has been investigated at zero bias voltage. The results show that, after functionalization of AGNR with PBASE, the conductance of the device increases while functionalization with probe and target DNA leads to a decrease in conductance. The changes in the projected density of states on the AGNR and transmission around Fermi energy are the reason for the change in conductance of the system. In all cases, both charge transfer and electrostatic gating are responsible for the change in the electrical properties of the system. The results show that our device detects DNA hybridization with a sensitivity of 10% at zero bias voltage, and by applying a suitable gate voltage, it can show higher sensitivity.

Keywords Graphene nanoribbon · Field effect transistor · DNA hybridization · Quantum transport · PBASE

Introduction

DNA is a biological molecule that contains the information of life hereditary. Therefore, recognizing the information coded in DNA is necessary for the prevention or treatment of diseases, personal medicine, and diagnostic of pathogenic or genetic diseases (Netto et al. 1990; Smith et al. 2020; Kowalczyk 2020). Thus, detection of not only a wide variety of infectious agents but also many genes that are responsible for inherited disease, demonstration of human chromosomal deviation, and demonstration of gene rearrangement and tumor cell identification can be possible with DNA hybridization (Smith et al. 2020). Moreover, nowadays, one of the most important applications of DNA hybridization can be the detection of severe acute respiratory syndrome coronavirus-2 (SARS-CoV-2) in order to prevent it from spreading before all people are vaccinated. Detection of SARS-CoV-2 is possible by hybridization

S. Bagherzadeh-Nobari (✉)
Department of Physics, Safadasht Branch, Islamic Azad University, Tehran, Iran
e-mail: sh.bagherzadeh@safaiau.ac.ir

R. Kalantarinejad
Hamava Innovation Factory, No. 31, Azadi Innovation Factory, Lashgari highway, Azadi square, Tehran, Iran

of RNA-dependent RNA polymerase gene (RdRp) of SARS-CoV-2 with the probe that has the reverse sequence of target (Thanihaichelvan et al. 2021; Hwang et al. 2021; Cheung et al. 2020). Traditional techniques of DNA hybridization show high sensitivity. But they come with some challenges and problems such as high cost and are time consuming (Milford Ward et al. 2001). Nowadays, nano filed effect transistor (FET) biosensors have attracted considerable attention (Bagherzadeh-Nobari et al. 2018a, 2020; Kalantari-Nejad et al. 2010) since they can be used as the label-free and real-time detection for biomolecules such as proteins, DNA, and bacteria (Thanihaichelvan et al. 2021; Kalantari-Nejad et al. 2010; Viswanathan et al. 2015; Bagherzadeh-Nobari et al. 2018b; Wu et al. 2018). Also, the fabrication of these FET biosensors is possible by some companies such as Graphenea (Fakih et al. 2019; Hayashi et al. 2020). In a FET DNA biosensor, the electrical properties of the FET such as source-drain current or conductance (G) of the channel change as a result of the attachment of complementary target DNA to the probe DNA immobilized on the channel surface. Therefore, detection can be observed due to doping of the channel by target DNA. Among different nano FET biosensors, graphene FET (GFET) biosensors have attracted considerable attention since graphene has advantages such as unique electrical properties, biocompatibility, and large detection area, and it is suitable for large-scale integrated device processing and fabrication due to planar geometry (Bagherzadeh-Nobari et al. 2018b; Wu et al. 2018; Xu et al. 2017; Ping et al. 2016).

There are some experimental studies that show that GFET DNA biosensors are a good candidate as a detector of DNA hybridization with high sensitivity, selectivity, stability, reproducibility, and reusability (Li et al. 2019; Mensah et al. 2020; Gao et al. 2020; Kim et al. 2020; Vishnubhotla et al. 2020; Zheng et al. 2015; Xu et al. 2018; Hwang et al. 2020).

As mentioned before, the mechanism of detection in GFET biosensors is based on a change in the transfer characteristics (source-drain current versus gate voltage). The instability of transfer characteristics makes the analysis of results hard. That is why the stability of transfer characteristics is very important. Transfer characteristics can be varied due to time, external environment, and transfer techniques due to contamination of graphene surface and damage.

Because GFET work in a solution environment, the stability of the device in the solution is very important for practical applications. There are some experimental studies that show the stability of GFET DNA biosensor in solution (Li et al. 2019; Mensah et al. 2020; Gao et al. 2020). For example, Li et al. (2019) fabricated a solution gated GFET DNA biosensor with high sensitivity. They proposed a novel method that probe DNA is placed on the gate electrode instead of the channel for target detection and they achieved the detection limit of femtomolar. They investigated the stability of the transfer characteristics of the sensor in the phosphate-buffered saline (PBS) solution over 6 h and showed that the transfer curve has only a little change at the first 2 h that is acceptable in the real application and does not change further over time that proves the stability of the sensor in solution environments.

In another work, Mensah et al. (2020) fabricated a GFET DNA biosensor with high sensitivity, specificity, and stable characteristics over 1 month. By using the innovation fabrication method and separating graphene from the electrolyte solution by thin insulator layer during hybridization and measurements, they reduced the electrochemical effects and contamination of graphene surface leading to instability of transfer characteristic of the device.

Gao et al. fabricated a high sensitive GFET DNA biosensor with a detection limit of 10 femtomolar without functionalization of graphene surface (Gao et al. 2020). They investigated the stability of the GFET sensor in PBS solution over 24 h and showed that change in transfer characteristics of the device is a bit due to the presence of ions and is negligible for real applications.

Kim et al. (2020) proposed an improved technique for the transfer of graphene on the substrate which reduces damage and doping effects. Thus, they fabricated a GFET DNA biosensor with high transfer characteristics stability.

Also, the reusability of the sensor is investigated in some experimental studies (Vishnubhotla et al. 2020; Zheng et al. 2015). For example, Xu et al. (2017) fabricated a multi-channel graphene biosensor with high stability, reusability, and sensitivity. Their sensor can be reused by removing the target DNA without dissociation of 1-pyrenebutanoic acid succinimidyl ester (PBASE) linker from graphene channel and without change in the density of probe DNA. Also, the

transfer curve is the same for forward and backward gate voltage sweeping that indicates the stability and reproducibility of the sensor.

In another work, Zheng et al. fabricated a FET DNA biosensor by a new directional transfer technique with high reusability and stability (Zheng et al. 2015). They investigated the reusability of their sensor by performing three-cycle hybridization and showed that hybridization signal after second and third times decreased 14% and 24%, respectively. Hence, their sensor shows good reusability. Also, their sensor is stable in PBS solution so that the change in transfer characteristics curve is negligible due to solution.

Recently, Vishnubhotla et al. fabricated a reusable GFET DNA biosensor with an attomolar detection limit (Vishnubhotla et al. 2020). Their sensor can be refreshed and reused multiple times by melting off bound target from probe without damaging the probe and with similar responses among multi-trials.

Although different experimental works indicate that graphene field effect transistors are a good candidate as a detector of DNA hybridization with high sensitivity and selectivity, they have not investigated the mechanism of detection and the reason for the change in the electrical properties of the device in presence of a linker, probe, and target DNA in detail (Xu et al. 2017; Ping et al. 2016). In spite of experimental study, we can theoretically reveal a reason for changes in the electrical properties and mechanism of detection by computing and analyzing the charge and electrostatic potential of the device, as the change in the electrical properties of a FET such as conductance is due to doping of the channel. Doping occurs directly by charge transfer between the target molecule and the channel and/or indirectly by electrostatic gating of the channel due to the presence of the target molecule. After doping, the amount of charge and/or the distribution of charge in the channel changes, and as a result, the conductance of the device changes.

Accordingly, for this purpose, we have modeled an armchair graphene nanoribbon (AGNR) interconnected between gold electrodes and investigated and compared the electrical properties of the device for bare AGNR, AGNR functionalized with PBASE, and AGNR functionalized with probe DNA via PBASE before (state (a)) and after (state (b)) hybridization with target DNA. In addition, the ability of the device

as a detector of DNA hybridization and the mechanism of detection is investigated.

Although in reality, there are some excess charges on the graphene surface due to the effect of the environment or substrate (Romero et al. 2008), we did not include them in our simulation since these charges do not have a significant effect on either detecting DNA hybridization or defining the mechanism of detection. These charges result in doping of graphene and accordingly result in a change in the conductance of the channel. Detection of DNA hybridization with complementary target DNA is observed due to the change in the conductance of the channel due to doping of channel by complementary target DNA while electrical properties of channel do not change in presence of non-complementary DNA. Therefore, we expect the initial charge carrier of the channel not to influence the distinguishability of complementary DNA from non-complementary DNA and the mechanism of detection.

The paper is organized as follows: First, in the "Simulation details and method" section, details of simulation of device and structure optimization are presented and then the theoretical method implemented is described. In the "Results and discussions" section, the electrical properties of the device such as projected density of states (PDOS) over the AGNR, transmission coefficient (T), and conductance at zero bias voltage for bare AGNR, AGNR functionalized with PBASE as well as for AGNR functionalized with probe DNA via PBASE linker before and after hybridization with target DNA are computed and compared. Also, in order to explore the underlying mechanism of the detection and reveal the reason for the changes in the electrical properties of the device, charge transfer and the electrostatic potential of the system are investigated. In the end, the paper is summarized in the last section.

Simulation details and method

We have used visual molecular dynamics (VMD) program (Humphrey et al. 1996) to build an armchair graphene nanoribbon having a length and width of 100 Å and 40 Å, respectively. Different experiments show that FET based on graphene functionalized with PBASE have high conductivity and sensitivity.

Functionalization with PBASE neither induces defects in the AGNR, nor changes the electrical and physical properties of AGNR (Xu et al. 2017; Ping et al. 2016; Kim et al. 2020; Vishnubhotla et al. 2020; Béraud et al. 2021; Hao et al. 2020; Fernandes et al. 2019; Tsang et al. 2019; Mudusu et al. 2020; Xia et al. 2021; Tian et al. 2020, 2018; Ohno et al. 2013; Guo et al. 2011; Wu et al. 2015, 2017; Gao et al. 2018; Forsyth et al. 2017). Based on these results, we have functionalized AGNR with PBASE. PBASE binds to the graphene surface non-covalently via the stacking of its pyrene group. Afterward, single-strand DNA (ssDNA) immobilized on the AGNR surface using binding to PBASE linker covalently. Bonding of probe DNA to the PBASE involves nucleophilic substitution N-hydroxysuccinimide by an amine group of probe DNA resulting in the formation of an amide bond. Figure 1 represents the structure of PBASE before and after binding to the ssDNA. The structure of DNA and PBASE is obtained from 3DART and Chemspider, respectively (Dijk and Bonvin 2009; Kim et al. 2016). We have used A chain

of the double-strand DNA (dsDNA) as probe DNA and B chain of the dsDNA as target DNA. Now, we need to obtain the optimized structure of the system. For this purpose, the minimization function of NAMD package that is based on conjugated gradient method is used (Phillips et al. 2005).

In NAMD software, CHARMM force field is implemented (MacKerell et al. 1998). The minimization process is as follows: first partial charge of the ssDNA linked to the PBASE is obtained by SIESTA code (Soler et al. 2002). Then, AGNR functionalized with probe DNA via PBASE linker is solvated in parallel piped water box with the dimension of $40.20 \times 102 \times 102$ Å^3. Na$^+$ ions are added in order to neutralize the charge of the system. The initial distance between carbon atoms of pyrene in PBASE and AGNR is set to 3 Å. Energy minimization is carried out until the energy of the system reaches a stable point. After minimization, the minimum distance between AGNR and PBASE becomes 3.6 Å. Finally, we put target DNA adjacent to the probe DNA and minimize the system in water and ions again. The

Fig. 1 Structure of (**a**) PBASE and (**b**) probe DNA bonded to the PBASE. Color code: light blue = C, dark blue = N, red = O, white = H, tan = P
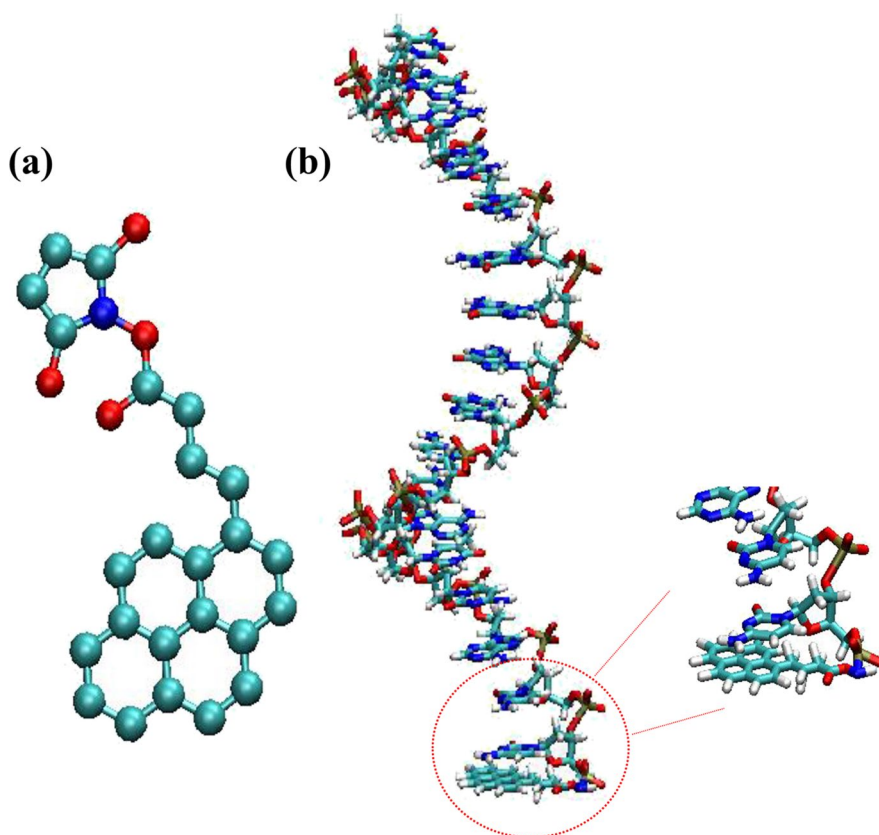
optimized structure of the system before and after DNA hybridization is shown in Fig. 2.

Then, the coordinates of the optimized structures are used for quantum transport calculations (Datta 1997). Due to the computational cost, water and ions are omitted for quantum transport calculations. In general, the biological environments have two effects on the electrical properties of the system. On one hand, the geometry of the target molecule changes due to thermal motion in the solvent leading to changes in the electrical properties of the system. On the other hand, in the systems comprising polar molecules, solvent surrounds the molecules and acts as an external gate. There are some theoretical works that have investigated the effect of water on the electrical properties of the system. For example, Song et al. (2012) investigated the effect of water on the detection of nucleotides using AGNR interconnected between Au electrodes and showed that in spite of the change in the geometry of nucleotides due to the thermal motion, detection is robust. In another work, Rungger et al. (2010) investigated the effect of water on the electrical properties of polar and non-polar systems and showed that only in the case of polar molecules, water acts as electrostatic gating and shifts the transmission of the device rigidly.

Since electrostatic gating arising from solvent is applied to both states (state (a) and (b)), we do not expect it to influence the contrast between the transport properties of the device before and after DNA hybridization as well as the mechanism of detection.

In order to simulate a FET biosensor and show the effect of linker, probe, and target DNA on the electrical properties of the device and define the mechanism of detection, we have placed AGNR between gold electrodes and computed the electrical properties of the system for bare AGNR, AGNR functionalized with PBASE, and AGNR functionalized with PBASE in presence of probe DNA before and after hybridization with target DNA. For this purpose, SMEA-GOL code (Rungger and Sanvito 2008) is used that combines non-equilibrium Green's function (NEGF) with density functional theory (DFT) (Hohenberg and Kohn 1964). For quantum transport calculations, our device is divided into the central region, left, and right electrodes (Fig. 3). The semi-infinite gold electrodes are periodic in the transport direction (z-direction). We have considered two Au layers into the central region in order to eliminate surface effects such as charge transfer or geometrical reconstruction of the electrodes due to the bonding to the graphene nanoribbon and screen bulk electrodes from the central region. As a result, we can ensure the similarity between charge density and effective potential of the electrodes and bulk structure. After partitioning the open system into three parts, the Hamiltonian of the system is presented as follows:
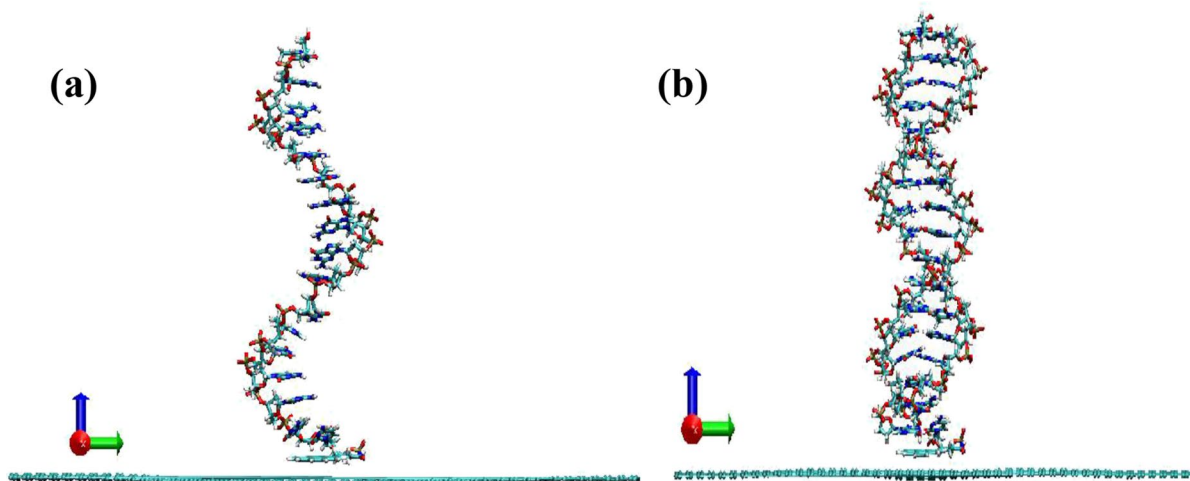

(a)   **(b)**

Fig. 2 Optimized structure of AGNR functionalized with probe DNA via PBASE (**a**) before and (**b**) after hybridization with target DNA. The sequence of probe DNA and target DNA are $5' - NH_2$ *CCA CTA CCG GGG CAC GT*$3'$ *and* $5' - ACG$ *TGC CCC GGT AGT GGT* $- 3'$, respectively. Color code: light blue = C, dark blue = N, red = O, white = H, tan = P

Fig. 3 Schematic illustration of the FET biosensor. The central region includes a portion of the infinitely long electrodes and graphene nanoribbon. The distance between Au electrodes and AGNR is 2 Å. Scale bar is 10 Å
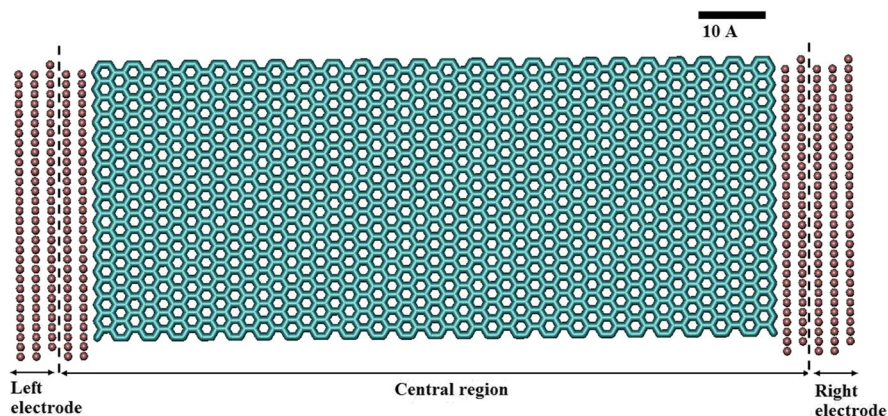
$$\begin{pmatrix} H_L & H_{LC}^{\dagger} & 0 \\ H_{CL} & H_C & H_{CR}^{\dagger} \\ 0 & H_{RC} & H_R \end{pmatrix} \tag{1}$$

where H_L, H_C, and H_R are Hamiltonian of the left electrode, central region, and the right electrode, respectively. Other non-zero elements of Hamiltonian matrix are interaction matrix between electrodes and the central region.

In order to solve Schrodinger equation, by using NEGF approach, we converted the infinite dimensional Hamiltonian of the system to the dimension of the central region. In this approach, retarded Green's function is defined as follows:

$$[E^+S - H]G = I \tag{2}$$

where $E^+ = \lim_{\varepsilon \to 0^+} E + i\varepsilon$, S is an overlap matrix, and I is identity matrix. By substitution of Hamiltonian of the system in this equation and performing some algebra, we can focus on the Green's function of the central region that is defined as follows:

$$G_C = \left[E^+S_C - H_C - \Sigma_L(E) - \Sigma_R(E)\right]^{-1} \tag{3}$$

so that G_C includes all the effects of electrodes as self-energy ($\Sigma_L(E)$ and $\Sigma_R(E)$) (Rocha et al. 2005).

As mentioned before, DNA hybridization can be detected by the change in the conductance of the channel. Hence, our main aim from quantum transport calculations is to obtain conductance that is proportional to the transmission. Transmission is defined as the probability of electrons with energy E going from one electrode through the channel to another electrode. It can be written as follows:

$$T(E) = \mathrm{Tr}\left[\Gamma_L G_C \Gamma_R G_C^{\dagger}\right] \tag{4}$$

where $\Gamma_{L,R}$ are coupling matrices which are defined as $\Gamma_{L,R} = i\left[\sum_{L,R} - \sum_{L,R}^{\dagger}\right]$ (Fisher and Lee 1981).

Local density approximation (LDA) in Ceperley-Alder form is used as the exchange–correlation functional in DFT calculations (Ceperley and Alder 1980). To model core electrons, Troullier and Martins norm-conserving pseudopotentials are implemented (Troullier and Martins 1991). For the real space grid, mesh cutoff of 200 Ryd is used. Due to the computational cost, single zeta basis set is implemented for carbon atoms of AGNR. A single zeta-polarized basis set is used for all atoms of DNA and PBASE. According to a well-tested strategy for Au atoms, we have considered d orbital as core and 6S shell as the valence (Toher and Sanvito 2008). For electrode calculations, Monkhorst pack of $1 \times 1 \times 30$ and for the device region Γ point is used.

Supercell has a dimension of $50.26 \times 80 \times 125.88$ Å^3 that consists of 2682, 2721, 3257, and 3797 atoms in the case of bare AGNR, AGNR functionalized with PBASE, state (a), and state (b), respectively.

The periodic boundary condition is applied in the directions transverse to the transport direction. We have considered the vacuum pad of 10 Å to avoid the interaction between the actual simulation box and its repeating image.

Results and discussions

First, we have analyzed the effect of the PBASE molecule on the electrical properties of AGNR

interconnected between gold electrodes. For this purpose, we have conducted and compared the PDOS and T as a function of energy for bare AGNR and AGNR functionalized with PBASE molecule at zero bias voltage (Fig. 4(a) and (b), respectively). The zero of the energy scale is set to the Fermi energy of electrodes. Knowing the fact that at zero bias voltage and room temperature, the states in the energy range

between ± 0.2 eV around Fermi energy are collaborative in the conduction; we have concentrated on the PDOS and T diagram in the energy range of ± 0.3 eV.

According to the PDOS diagram (orange line in Fig. 4(a)), AGNR interconnected between gold electrodes is a degenerate n-type semiconductor due to the fact that the conduction band edge is located at -0.0113 eV below Fermi energy. There are some

Fig. 4 (**a**) The PDOS and (**b**) T diagrams of bare AGNR (orange line) and AGNR functionalized with PBASE (blue line). T is plotted in logarithmic scale
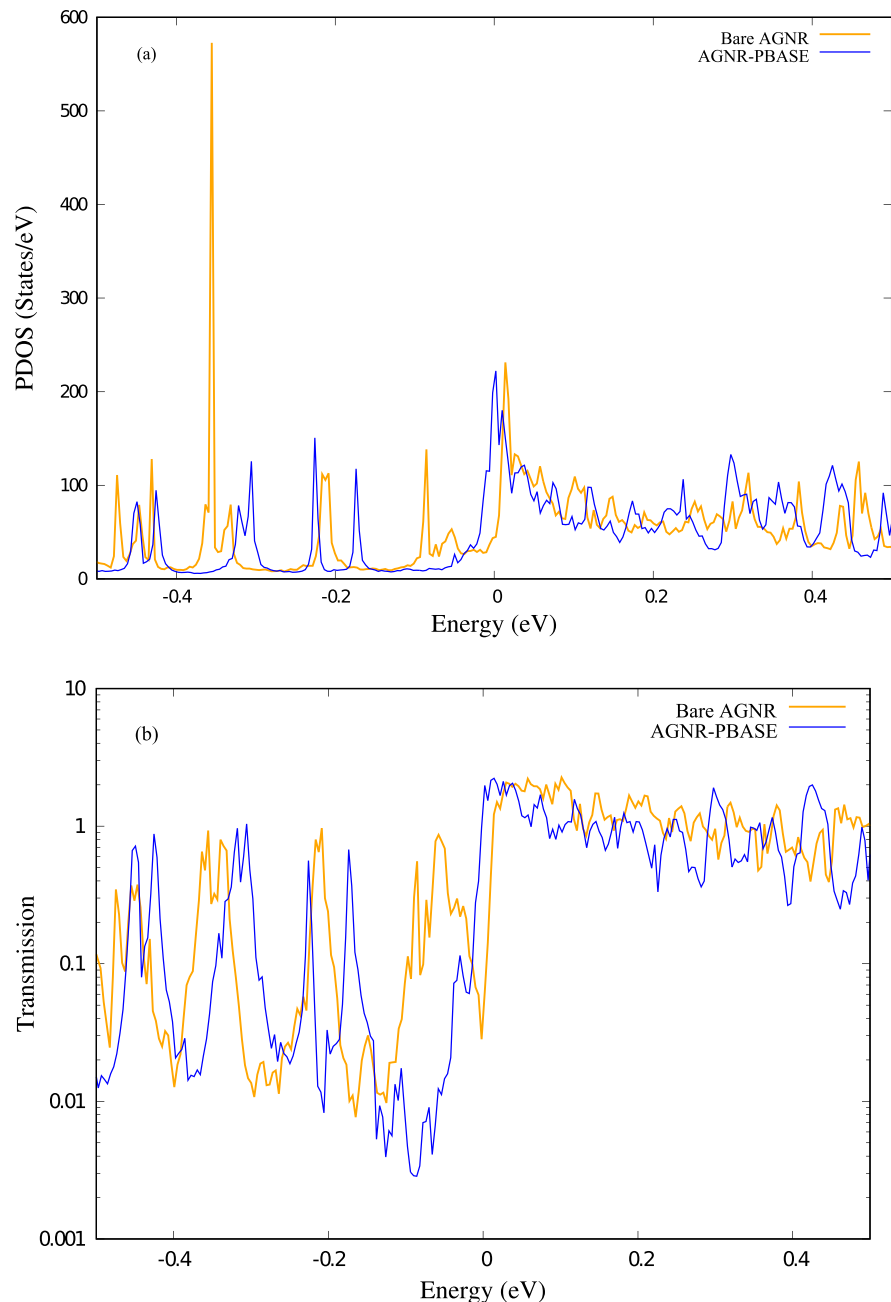
peaks in the band-gap region going from -0.0113 eV to lower energies known as metal-induced gap states. These states can be ascribed to interface states due to the presence of metal contacts and cause tunneling of electrons through the channel (Tersoff 1984; O Odbadrakh 2007).

By cross-checking the PDOS diagram with the T diagram (orange line in Fig. 4(b)), we can conclude that there is good comply between them so that the transmission coefficient of conduction band going from -0.0113 eV to higher energies is about 1.5, and in the band-gap region, we can see non-zero transmission arising from mid-gap states in the band-gap region that causes mid-gap tunneling conductance. Also, there are not any localized states in the PDOS diagram that lead to a reduction in the transmission coefficient.

Functionalization of AGNR with PBASE molecule brings about a general shift of PDOS to lower energies (blue line in Fig. 4(a)). Such a shift is more significant in the band-gap region which now a double peak composed of a broaden peak at -0.054 eV and a sharp peak at -0.08 eV shift to energies of -0.174 eV and -0.227 eV, respectively, and two closely spaced sharp peaks around -0.21 eV move to -0.316 eV. As such, after the functionalization of AGNR with PBASE molecule, the conduction band edge shifts downward from -0.0113 to -0.002 eV. Such a shift is due to the emergence of new states at the conduction band edge and the overall shift of PDOS to lower energies.

We guess that the increase in the states near the conduction band edge can be due to increase in the majority charge carriers (in this case electrons), and the downward shift of the PDOS can be due to electrostatic gating of AGNR.

According to Fig. 4(a) and (b) (blue line), there is a good comply between PDOS and the transmission coefficient, so that, after functionalization of AGNR with PBASE, transmission onset at the conduction band moves from -0.0113 to -0.002 eV and we can see a general downward shift of the transmission to lower energies.

In order to validate our claims and reveal the reason for the change in the PDOS and T, the charge and electrostatic potential of the system are computed and compared before and after functionalization with PBASE. The charge of the system is conducted by Mulliken population analysis. The

results are summarized in Table 1. The results show that after functionalization with PBASE molecule, the significant charge is transferred to the AGNR, leading to enhancement in majority charge carriers in the n-type degenerate AGNR. On account of increase in majority charge carriers, new states appear at the conduction band edge and AGNR becomes more metallic. We can justify such a charge transfer as a result of interaction between p-orbitals residing on the pyrene group and delocalized π-electrons on AGNR (Song et al. 2012; Karachevtsev et al. 2011; Fan and Zhang 2008). There are some experimental and theoretical works that indicate charge transfer occurs from pyrene to carbon nanotubes (Karachevtsev et al. 2011; Fan and Zhang 2008). But experimental studies on GFET functionalized with PBASE showed that charge transfer occurs from graphene to PBASE (Xu et al. 2018; Ohno et al. 2013). Recently, Hinnemo et al. investigated the adsorption of PBASE on the graphene surface (Hinnemo et al. 2017). They showed that when the number of PBASE molecules on the surface is low, pyrene group in PBASE places horizontally on graphene surface (similar to our work) while by increasing the number of PBASE molecules, due to strong interaction between PBASE with graphene and other PBASE molecules, pyrene group places relatively vertically. So, we can conjecture such a difference in charge transfer is related to the different configurations of PBASE with respect to AGNR.

Afterward, the electrostatic potential of the system is computed and plotted using plrho utility that is implemented in the SIESTA code. First, the isosurface of charge density is plotted for specific isovalue and is colored according to the electrostatic potential of the system. First, we have analyzed the electrostatic potential of bare AGNR (Fig. 5(a)). As demonstrated in the figure, the electrostatic potential of AGNR near the electrodes is higher (light blue color) in comparison to other regions (red

Table 1 Charge difference in AGNR. The charge of the system is computed by Mulliken pop analysis. The negative sign means charge loosing and positive sign means charge achieving

Channel	AGNR-PBASE	State (a)	State (b)
ΔQ	$+3.251e$	$-0.49e$	$-0.266e$

Fig. 5 Electrostatic potential of (**a**) bare AGNR and (**b**) AGNR-PBASE. The value of coloring function of electrostatic potential is determined with blue, white, and red that are related to the maximum, mean, and minimum saturation range of electrochemical potential. Isosurfaces are plotted for isovalue of $10^{-4} \frac{e}{bohr^{-3}}$
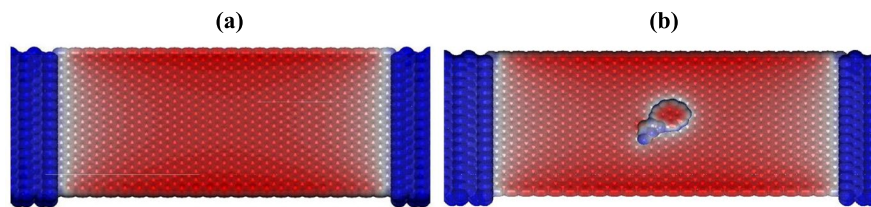
	Potential	
	AGNR	**AGNR-PBASE**
Blue	0.050	0.776
White	-0.051	0.035
Red	-0.108	-0.0656

Table 2 Conductance of FET biosensor at different states

Channel	Bare AGNR	AGNR-PBASE	State (a)	State (b)
Conductance (G_0)	0.04	1.47	0.73	0.65

color). Such an increase corresponds to the n-doping of AGNR due to the presence of electrodes.

Then, we have analyzed the electrostatic potential of AGNR in presence of PBASE molecule (Fig. 5(b)). According to the figure, after functionalization of AGNR with PBASE, the electrostatic potential of AGNR close to the PBASE increases due to the accumulation of negative charge in these regions (blue regions). Charge accumulation in AGNR occurs directly as a result of significant charge transfer to it and indirectly due to the presence of PBASE that now has positive charge due to charge losing and acts as a positive electrostatic gate.

These results prove our guess about the reason for the change in the PDOS and T diagrams. So that due to positive electrostatic gating of AGNR, PDOS, and as a result, T shift to lower energies.

Finally, the conductance of the system is computed before and after functionalization of AGNR with PBASE at zero bias voltage, and the results are mentioned in Table 2. At small gate voltages, the relation between transmission and conductance is defined by the expression $G(V_g) = G_0 T(E = \mu)$, where $G_0 = 2e^2/h$ is quantum of conductance and $\mu = E_F - eV_g$ is the electrochemical potential that can be tuned by applying a gate voltage, V_g (Leão De Souza et al. 2017). We have computed the electrical properties of the device at zero bias voltage without applying any gate voltage. Therefore, conductance can be obtained by the product of quantum of conductance and transmission evaluated at Fermi energy of electrodes, $T(E_F)$.

As set out in the table, after functionalization with PBASE, the conductance of the system increases considerably. The increase of conductance is related to the increase of states and as a result T around Fermi energy that has a major role in conductance at zero bias voltage. As mentioned before, the increase in the PDOS around Fermi energy is because of n-doping of AGNR that causes Fermi level cuts through the bottom of the conduction band edge and AGNR becomes more metallic.

Now, we scrutinize and analyze the effect of immobilization of probe DNA on the electrical properties of AGNR interconnected between gold electrodes at zero bias voltage. For this purpose, we have conducted and compared the PDOS and T as a function of energy for AGNR functionalized with PBASE in the absence and presence of probe DNA at zero bias voltage (blue and green lines in Fig. 6(a) and (b), respectively). In order to show the changes of PDOS and T around Fermi energy more clearly, we have plotted them in the energy range -0.03 and 0.03 eV (Fig. 7(a) and (b)), respectively.

According to the PDOS diagrams (green line in Fig. 6(a) and 7(a)), functionalization of the channel with probe DNA causes the shift of PDOS to higher energies. Such a shift is significant in the band-gap region so that localized peaks located at -0.174 eV and -0.227 eV shift by about 0.03 eV upward and two closely spaced sharp peaks located at -0.30 eV and -0.32 eV shift to -0.284 eV and -0.29 eV,

Fig. 6 (a) The PDOS and (b) *T* diagrams of AGNR functionalized with PBASE (blue line), state (a) (green line), and state (b) (red line). *T* is plotted in logarithmic scale
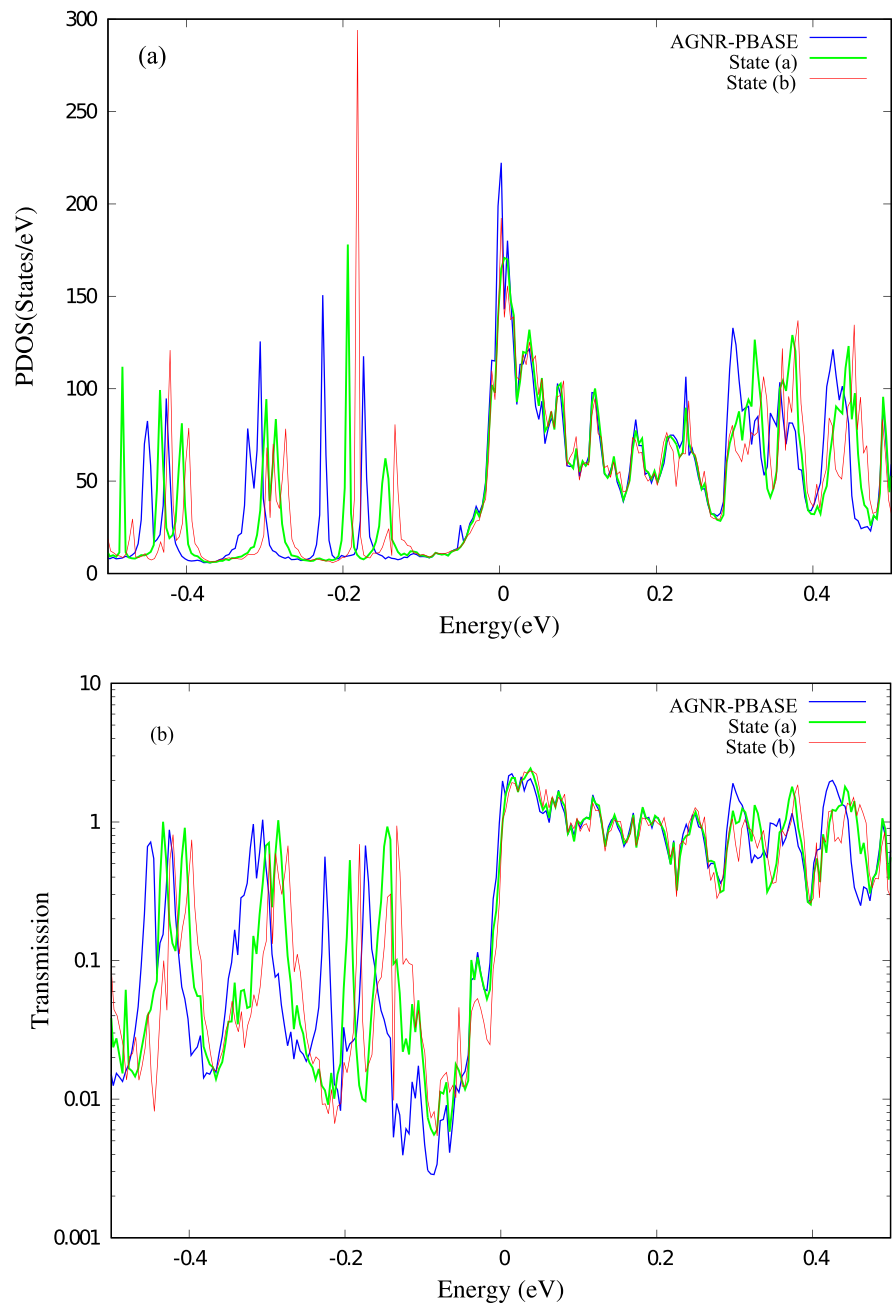

respectively. Also, the conduction band changes significantly so that the highest peak at the conduction band around E_F shifts slightly upward from 0.002 to 0.006 eV. As such, we can see a decrease in states at the conduction band edge and around Fermi energy.

By cross-checking of the PDOS with *T* diagrams (green line in Fig. 6(b) and 7(b)), we can find that the changes in the PDOS after immobilization of

probe DNA are reflected into the *T* diagram. So that after functionalization with probe DNA, we can see a general upward shift of the transmission to higher energies that is significant in the band-gap region. Also, due to a decrease in states near the conduction band edge and around Fermi energy, transmission decreases in these energies.

Fig. 7 (a) The PDOS and
(b) T diagrams of AGNR
functionalized with PBASE
(blue line), state (a) (green
line), and state (b) (red
line) zoomed in the energy
range -0.03–0.03 eV. T is
plotted in logarithmic scale
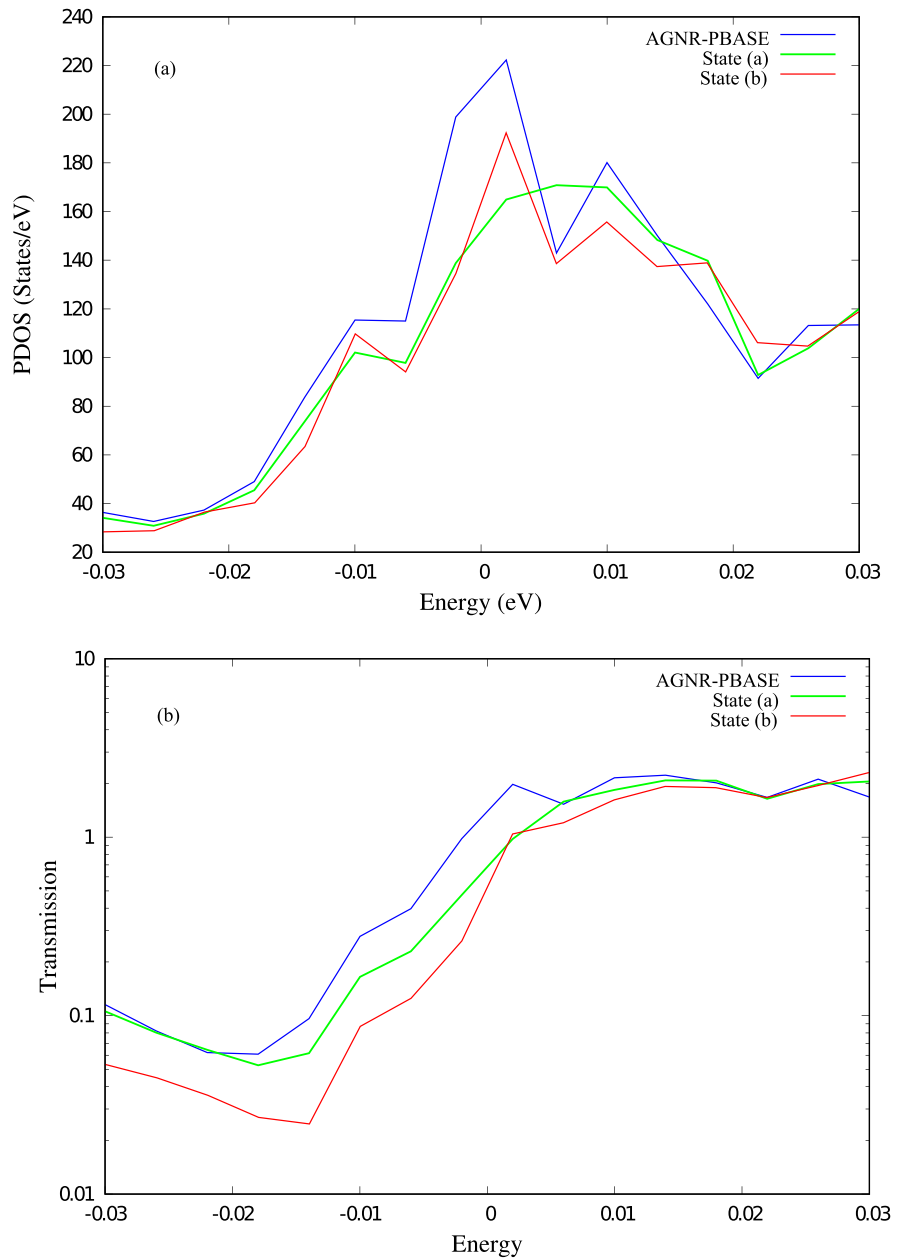
In order to find the reason for the change in electrical properties of the device, the charge transfer and electrostatic potential of the system are computed and compared before and after functionalization with probe DNA. The results are depicted in Table 1 and Fig. 8(a). As set out in the table, AGNR in presence of probe DNA loses charge. On account of mirror charge transfer, the conduction band edge does not change considerably. Also, we conjecture

the decrease in states at the conduction band edge is because of the decrease in majority charge carriers (electrons).

Now, we scrutinize and analyze how probe DNA affects the electrostatic potential of the device. In comparison with the electrostatic potential of AGNR functionalized with PBASE molecule, we can see that functionalization with probe DNA (Fig. 8(a)) leads to depletion of charge (accumulation of positive

Fig. 8 Electrostatic potential of device for (a) state (a) and (b) state (b) from top and side view. The value of coloring function of electrostatic potential is determined with blue, white, and red that are related to the maximum, mean, and minimum saturation range of electrochemical potential. Isosurfaces are plotted for isovalue of $10^{-4} \frac{e}{bohr^{-3}}$
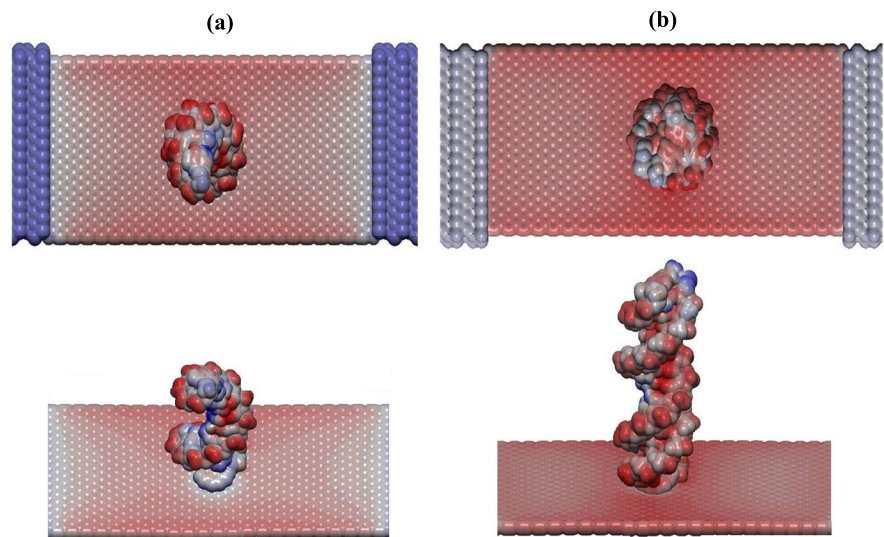
	Potential	
	State (a)	**State (b)**
Blue	0.148	-0.03
White	-0.073	-0.14
Red	-0.191	-0.346

charge) and, as a result, a decrease in the electrostatic potential of AGNR in the vicinity of probe DNA (in these regions, electrostatic potential changed from dark blue to light blue). The depletion of charge on the AGNR is because of charge losing and negative electrostatic gating in the presence of probe DNA. Therefore, we can conclude that due to the negative electrostatic gating of the device, PDOS and T should shift to higher energies that are consistent with our previous findings.

Then, we have computed the conductance of the device after immobilization of probe DNA on the AGNR surface at zero bias voltage. The result is mentioned in Table 2. We can observe that after immobilization of probe DNA on the AGNR surface, the conductance of the device decreases. Such a decrease is because of the decrease of states and consequently T around Fermi energy. As mentioned before, the decrease in majority charge carriers and shift of PDOS to higher energies lead to the reduction of states around Fermi energy.

Afterward, we have investigated the effect of hybridization of DNA on the electrical properties of the device at zero bias voltage. First, we have analyzed the change in the PDOS and T diagrams after DNA hybridization. For this purpose, we have plotted the PDOS and T of the device before and after DNA hybridization (green and red lines in Fig. 6(a) and (b), respectively). In order to depict the changes of PDOS and T around Fermi energy more clearly, we have plotted them in the energy range -0.03 and 0.03 eV (Fig. 7(a) and (b), respectively).

As can be observed from Fig. 6(a) and 7(a) (red line), there are significant changes in the PDOS diagram after DNA hybridization. We can see a shift of the PDOS toward higher energies that is significant in the band-gap region in a way that all the peaks in the band-gap region shift upward by about 0.1 eV. By looking at the conduction band, we can see that after DNA hybridization, the conduction band edge moves slightly upward and we can observe the reduction of the states at the conduction band edge around -0.03 eV. As such, we can see an increase in PDOS around Fermi energy.

Afterward, we have analyzed the effect of DNA hybridization on the transmission coefficient of the system (red line in Fig. 6(b) and 7(b)). As depicted in figures, after DNA hybridization, the onset of transmission at the conduction band shifts slightly upward, and due to the decrease in states at the conduction band edge, transmission decreases in these energies.

As such, despite the increase in PDOS around Fermi energy after DNA hybridization, transmission decreases. Therefore, we can conclude that these new states are localized states which scatter electrons and result in a decrease in the transmission.

In order to find the mechanism of detection and the reason for the change in the electrical properties of the device, hereafter, we will investigate the change in the charge and electrostatic potential of the sensor after DNA hybridization.

First, we have computed the charge of the device after DNA hybridization. The results are mentioned in Table 1. According to the table, mirror charge is transferred from AGNR after DNA hybridization. Accordingly, majority charge carriers (electrons) decrease due to the fact that AGNR interconnected between gold electrodes is an n-type semiconductor.

Then, we have analyzed the electrostatic potential of the device after DNA hybridization (Fig. 8(b)). By comparing the electrostatic potential of the device in states (a) and (b), we can realize that target DNA causes further charge depletion in the channel and, as a result, a decrease in electrostatic potential. Charge losing and negative charge of DNA molecule is the reason for depletion of charge in the AGNR.

Now, we can reveal the reason for the changes in the PDOS and T diagrams. According to our findings, both charge transfer and electrostatic gating contribute to the change in the electrical properties of the device. In fact, because of the negative electrostatic gating of AGNR, the PDOS and the T shift to higher energies. As such, the reduction of the PDOS at the conduction band edge is related to the decrease of majority charge carriers (electrons).

Then, we have computed the conductance of the device after DNA hybridization at zero bias voltage. The results are mentioned in Table 2. As can be observed from the table, DNA hybridization causes a reduction in conductance from 0.73 to 0.65 G_0. As a result, detection of DNA hybridization can be possible. A decrease in conductance is due to decrease of T around Fermi energy.

Finally, the sensitivity of the sensor is computed using the formula $S = \frac{G - G_0}{G_0} \times 100$, where G_0 and G represent conductance of the sensor before and after DNA hybridization, respectively. Based on our findings, our device shows a sensitivity of 10% at zero

bias voltage. Due to the fact that at small bias voltages, the electronic structure of the device does not change significantly compared to zero bias voltage; we can conclude from our PDOS and T diagrams that due to considerable changes in the band-gap region after DNA hybridization, we expect at higher bias voltages (wider energy window), and by applying a suitable gate voltage, mid-gap states contribute to conductance, and the device can show more sensitivity (Leão De Souza et al. 2017) and can be used as an effective DNA hybridization detector.

Conclusion

In this study, we have modeled an AGNR interconnected between gold electrodes as a DNA hybridization detector and have investigated the sensing ability of the device at zero bias voltage. Also, we have computed the electrical properties of the device such as PDOS, T, and conductance at zero bias voltage for bare AGNR, AGNR functionalized with PBASE, and AGNR functionalized with probe DNA via PBASE molecule before and after DNA hybridization with the complementary part. In order to find the reason for the change in the electrical properties of the device and reveal the mechanism of detection, the charge transfer and the electrostatic potential of the device are computed and analyzed. The results show that after the functionalization of AGNR with PBASE, a significant charge is transferred to AGNR that causes an increase in the majority charge carriers. Charge transfer to AGNR and positive electrostatic gating of AGNR in presence of positively charged PBASE lead to charge accumulation in the channel and, as a result, an increase in the electrostatic potential in AGNR in the vicinity of PBASE molecule. The appearance of new states around Fermi energy due to charge transfer and shift of PDOS to lower energies due to positive electrostatic gating cause an increase in PDOS and as a result T around Fermi energy ultimately leading to conductance increase at zero bias voltage. After functionalization with probe DNA, AGNR loses mirror charge. Due to the presence of negative charge of probe DNA and charge losing, charge depletion occurs on the channel and the electrostatic potential of these regions decreases in comparison to the other regions. Further decrease in the electrostatic potential of AGNR is seen due to further

charge transfer from AGNR and negative charge of target DNA. The results show that in both cases (state (a) and (b)), PDOS and T shift to higher energies due to negative electrostatic gating. Also, functionalization with probe and target DNA causes a decrease in conductance at zero bias voltage due to a decrease in T around Fermi energy. Based on our findings, our device can detect DNA hybridization with a sensitivity of 10% at zero bias voltage. But due to the fact that PDOS and T show a significant change in the band-gap region after DNA hybridization, we can conclude that at higher bias voltages and by applying a suitable gate voltage (where mid-gap states have a major role in the conductance of the system), our device can be more sensitive and can be used as a good candidate for DNA hybridization detector.

Availability of data and material All data generated or analyzed during this study are included in this published article.

Code availability Smeagol code is used in this publication that is available free of charge for researchers belonging to Academic community.

Declarations

Conflict of interest The authors declare no competing interests.

References

Bagherzadeh-Nobari S, Hosseini-Istadeh K, Kalantarinejad R et al (2018a) Computational investigation of single-wall carbon nanotube functionalized with palladium nanoclusters as hydrogen sulfide gas sensor. Int Nano Lett 8:9–15. https://doi.org/10.1007/s40089-018-0226-6

Bagherzadeh-Nobari S, Kalantarinejad R, Elahi SM, Sanvito S (2018b) Computational investigation of label free detection of biomolecules based on armchair graphene nanoribbon. Sensors Actuators B Chem 255:1276–1284. https://doi.org/10.1016/j.snb.2017.08.113

Bagherzadeh-Nobari S, Hosseini-Istadeh K, Kalantarinejad R (2020) Computational modelling of an amide functionalized single-walled carbon nanotube based H2S gas sensor. Phys E Low-Dimensional Syst Nanostructures 115:113691. https://doi.org/10.1016/j.physe.2019.113691

Béraud A, Sauvage M, Bazán CM et al (2021) Graphene field-effect transistors as bioanalytical sensors: Design, operation and performance. Analyst 146:403–428. https://doi.org/10.1039/D0AN01661F

Ceperley DM, Alder BJ (1980) Ground state of the electron gas by a stochastic model. Phys Rev Lett 45:566–569. https://doi.org/10.1103/PhysRevLett.45.566

Cheung KM, Abendroth JM, Nakatsuka N et al (2020) Detecting DNA and RNA and differentiating single-nucleotide variations via field-effect transistors. Nano Lett 20:5982–5990. https://doi.org/10.1021/acs.nanolett.0c01971

Datta S (1997) Electronic transport in mesoscopic systems. Cambridge University Press, Cambridge

Fakih I, Centeno A, Zurutuza A et al (2019) High resolution potassium sensing with large-area graphene field-effect transistors. Sensors Actuators B Chem 291:89–95. https://doi.org/10.1016/j.snb.2019.04.032

Fan W, Zhang R (2008) Structural and electronic properties of single-walled carbon nanotubes adsorbed with 1-pyrenebutanoic acid, succinimidyl ester. Sci China Ser B Chem 51:1203–1210. https://doi.org/10.1007/s11426-008-0140-2

Fernandes E, Cabral PD, Campos R et al (2019) Functionalization of single-layer graphene for immunoassays. Appl Surf Sci 480:709–716. https://doi.org/10.1016/j.apsusc.2019.03.004

Fisher DS, Lee PA (1981) Relation between conductivity and transmission matrix. Phys Rev B 23:6851–6854. https://doi.org/10.1103/PhysRevB.23.6851

Forsyth R, Devadoss A, Guy OJ (2017) Graphene field effect transistors for biomedical applications: current status and future prospects. Diagnostics 7:45. https://doi.org/10.3390/diagnostics7030045

Gao Z, Xia H, Zauberman J et al (2018) Detection of sub-fM DNA with target recycling and self-assembly amplification on graphene field-effect biosensors. Nano Lett 18:3509–3515. https://doi.org/10.1021/acs.nanolett.8b00572

Gao J, Gao Y, Han Y et al (2020) Ultrasensitive label-free MiRNA sensing based on a flexible graphene field-effect transistor without functionalization. ACS Appl Electron Mater 2:1090–1098. https://doi.org/10.1021/acsaelm.0c00095

Guo SR, Lin J, Penchev M et al (2011) Label free DNA detection using large area graphene based field effect transistor biosensors. J Nanosci Nanotechnol 11:5258–5263. https://doi.org/10.1166/jnn.2011.3885

Hao Z, Pan Y, Huang C et al (2020) Modulating the linker immobilization density on aptameric graphene field effect transistors using an electric field. ACS Sensors 5:2503–2513. https://doi.org/10.1021/acssensors.0c00752

Hayashi CK, Garmire DG, Yamauchi TJ et al (2020) High on-off ratio graphene switch via electrical double layer gating. IEEE Access 8:92314–92321. https://doi.org/10.1109/access.2020.2994611

Hinnemo M, Zhao J, Ahlberg P et al (2017) On Monolayer formation of pyrenebutyric acid on graphene. Langmuir 33:3588–3593. https://doi.org/10.1021/acs.langmuir.6b04237

Hohenberg P, Kohn W (1964) Inhomogeneous electron gas. Phys Rev 136:B864. https://doi.org/10.1103/PhysRev.136.B864

Humphrey W, Dalke A, Schulten K (1996) VMD: visual molecular dynamics. J Mol Graph 14:33–38. https://doi.org/10.1016/0263-7855(96)00018-5

Hwang MT, Heiranian M, Kim Y et al (2020) Ultrasensitive detection of nucleic acids using deformed graphene

channel field effect biosensors. Nat Commun 11:1–11. https://doi.org/10.1038/s41467-020-15330-15339

Hwang C, Park N, Kim ES et al (2021) Ultra-fast and recyclable DNA biosensor for point-of-care detection of SARS-CoV-2 (COVID-19). Biosens Bioelectron 185:113177. https://doi.org/10.1016/j.bios.2021.113177

Kalantari-Nejad R, Bahrami M, Rafii-Tabar H et al (2010) Computational modeling of a carbon nanotube-based DNA nanosensor. Nanotechnology 21:445501. https://doi.org/10.1088/0957-4484/21/44/445501

Karachevtsev VA, Stepanian SG, Glamazda AY et al (2011) Noncovalent interaction of single-walled carbon nanotubes with 1-pyrenebutanoic acid succinimide ester and glucoseoxidase. J Phys Chem C 115:21072–21082. https://doi.org/10.1021/jp207916d

Kim S, Thiessen PA, Bolton EE et al (2016) PubChem substance and compound databases. Nucleic Acids Res 44:D1202–D1213. https://doi.org/10.1093/nar/gkv951

Kim HE, Schuck A, Oh J et al (2020) Improving the neutrality point uniformity for SG-FET-based DNA sensor. Solid State Electron 167:107750. https://doi.org/10.1016/j.sse.2019.107750

Kowalczyk A (2020) Trends and perspectives in DNA biosensors as diagnostic devices. Curr Opin Electrochem 23:36–41. https://doi.org/10.1016/j.coelec.2020.03.003

Leão De Souza FA, Scopel WL, Scheicher RH et al (2017) Electrical detection of nucleotides via nanopore in hybrid graphene/h-BN sheet. Nanoscale 9:2207–2212. https://doi.org/10.1039/C6NR07154F

Li S, Huang K, Fan Q et al (2019) Highly sensitive solution-gated graphene transistors for label-free DNA detection. Biosens Bioelectron 136:91–96. https://doi.org/10.1016/j.bios.2019.04.034

MacKerell AD, Bashford D, Bellott M et al (1998) All-atom empirical potential for molecular modeling and dynamics studies of proteins. J Phys Chem B 102:3586–3616. https://doi.org/10.1021/jp973084f

Mensah K, Cissé I, Pierret A et al (2020) DNA Hybridization Measured with Graphene Transistor Arrays. Adv Healthc Mater 9:2000260. https://doi.org/10.1002/adhm.202000260

Milford Ward A, Catto JWF, Hamdy FC et al (2001) Prostate specific antigen: biology, biochemistry and available commercial assays. Ann Clin Biochem 38:633–651. https://doi.org/10.1258/0004563011901055

Mudusu D, Nandanapalli KR, Lee S, Hahn YB (2020) Recent advances in graphene monolayers growth and their biological applications: a review. Adv Colloid Interface Sci 102225. https://doi.org/10.1016/j.cis.2020.102225

Netto GJ, Tawil AN, Newman JT, Savino DA (1990) DNA hybridization: current clinical applications. In: Baylor University Medical Center Proceedings. Taylor & Francis, pp 45–52. https://doi.org/10.1080/08998280.1990.11929739

Ohno Y, Okamoto S, Maehashi K, Matsumoto K (2013) Direct electrical detection of DNA hybridization based on electrolyte-gated graphene field-effect transistor. Jpn J Appl Phys 52:110107. https://doi.org/10.7567/JJAP.52.110107

O Odbadrakh K (2007) Theoretical investigations for molecular electronic devices: metal∕ semiconductor interfaces, capacitance of atomic scale wires, and organics on diamond surfaces. Dissertation, North Carolina State University

Phillips JC, Braun R, Wang WEI et al (2005) Scalable molecular dynamics with NAMD. J Comput Chem 26:1781–1802. https://doi.org/10.1002/jcc.20289

Ping J, Vishnubhotla R, Vrudhula A, Johnson ATC (2016) Scalable production of high sensitivity, label-free DNA biosensors based on back-gated graphene field effect transistors. ACS Nano 10:8700–8704. https://doi.org/10.1021/acsnano.6b04110

Rocha AR, García-SUÁREZ VM, Bailey SW et al (2005) Towards molecular spintronics. Nat Mater 4:335–339. https://doi.org/10.1038/nmat1349

Romero HE, Shen N, Joshi P et al (2008) n-type behavior of graphene supported on Si/SiO2 substrates. ACS Nano 2:2037–2044. https://doi.org/10.1021/nn800354m

Rungger I, Sanvito S (2008) Algorithm for the construction of self-energies for electronic transport calculations based on singularity elimination and singular value decomposition. Phys Rev B 78:035407. https://doi.org/10.1103/PhysRevB.78.035407

Rungger I, Chen X, Schwingenschlögl U, Sanvito S (2010) Finite-bias electronic transport of molecules in a water solution. Phys Rev B 81:235407. https://doi.org/10.1103/PhysRevB.81.235407

Smith R, Geary SM, Salem AK (2020) Silicon nanowires and their impact on cancer detection and monitoring. ACS Appl Nano Mater 3:8522–8536. https://doi.org/10.1021/acsanm.0c01572

Soler JM, Artacho E, Gale JD et al (2002) The SIESTA method for ab initio order-N materials simulation. J Phys Condens Matter 14:2745–2779. https://doi.org/10.1088/0953-8984/14/11/302

Song B, Cuniberti G, Sanvito S, Fang H (2012) Nucleobase adsorbed at graphene devices: enhance bio-sensorics. Appl Phys Lett 100:063101. https://doi.org/10.1063/1.3681579

Tersoff J (1984) Schottky barrier heights and the continuum of gap states. Phys Rev Lett 52:465–468. https://doi.org/10.1103/PhysRevLett.52.465

Thanihaichelvan M, Surendran SN, Kumanan T et al (2021) Selective and electronic detection of COVID-19 (Coronavirus) using carbon nanotube field effect transistor-based biosensor: a proof-of-concept study. Mater Today Proc. https://doi.org/10.1016/j.matpr.2021.05.011

Tian M, Xu S, Zhang J et al (2018) RNA detection based on graphene field-effect transistor biosensor. Adv Condens Matter Phys 2018. https://doi.org/10.1155/2018/8146765

Tian M, Qiao M, Shen C et al (2020) Highly-sensitive graphene field effect transistor biosensor using PNA and DNA probes for RNA detection. Appl Surf Sci 527:146839. https://doi.org/10.1016/j.apsusc.2020.146839

Toher C, Sanvito S (2008) Effects of self-interaction corrections on the transport properties of phenyl-based molecular junctions. Phys Rev B 77:155402. https://doi.org/10.1103/PhysRevB.77.155402

Troullier N, Martins JL (1991) Efficient pseudopotentials for plane-wave calculations. Phys Rev B 43:1993–2006. https://doi.org/10.1103/PhysRevB.43.1993

Tsang DKH, Lieberthal TJ, Watts C et al (2019) Chemically functionalised graphene FET biosensor for the label-free

sensing of exosomes. Sci Rep 9:1–10. https://doi.org/10.1038/s41598-019-50412-9

van Dijk M, Bonvin AMJJ (2009) 3D-DART: a DNA structure modelling server. Nucleic Acids Res 37:W235–W239. https://doi.org/10.1093/nar/gkp287

Vishnubhotla R, Sriram A, DIckens OO, et al (2020) Attomolar detection of ssDNA without amplification and capture of long target sequences with graphene biosensors. IEEE Sens J 20:5720–5724. https://doi.org/10.1109/JSEN.2020.2973949

Viswanathan S, Narayanan TN, Aran K et al (2015) Graphene-protein field effect biosensors: glucose sensing. Mater Today 18:513–522. https://doi.org/10.1016/j.mattod.2015.04.003

Wu G, Tang X, Meyyappan M, Lai KWC (2015) Chemical functionalization of graphene with aromatic molecule. IEEE-NANO 2015 - 15th Int Conf Nanotechnol 1324–1327. https://doi.org/10.1109/NANO.2015.7388878

Wu G, Tang X, Meyyappan M, Lai KWC (2017) Doping effects of surface functionalization on graphene with aromatic molecule and organic solvents. Appl Surf Sci 425:713–721. https://doi.org/10.1016/j.apsusc.2017.07.048

Wu G, Meyyappan M, Wai Chiu Lai K (2018) Simulation of graphene field-effect transistor biosensors for bacterial detection. Sensors 18:1715. https://doi.org/10.3390/s18061715

Xia Y, Sun Y, Li H et al (2021) Plasma treated graphene FET sensor for the DNA hybridization detection. Talanta 223:121766. https://doi.org/10.1016/j.talanta.2020.121766

Xu S, Zhan J, Man B et al (2017) Real-time reliable determination of binding kinetics of DNA hybridization using a multi-channel graphene biosensor. Nat Commun 8:14902. https://doi.org/10.1038/ncomms14902

Xu S, Jiang S, Zhang C et al (2018) Ultrasensitive label-free detection of DNA hybridization by sapphire-based graphene field-effect transistor biosensor. Appl Surf Sci 427:1114–1119. https://doi.org/10.1016/j.apsusc.2017.09.113

Zheng C, Huang L, Zhang H et al (2015) Fabrication of ultrasensitive field-effect transistor DNA biosensors by a directional transfer technique based on CVD-grown graphene. ACS Appl Mater Interfaces 7:16953–16959. https://doi.org/10.1021/acsami.5b03941